Engineering Science and Technology, an International Journal 22 (2019) 801–810

HOSTED BY

Contents lists available at ScienceDirect

Engineering Science and Technology, an International Journal

journal homepage: www.elsevier.com/locate/jestch

Full Length Article

Enhancing FRT performance and smoothing output power of DFIG wind farm equipped by SFCL and SMES in a fuzzy framework

Mostafa Sedighizadeh [a,*], Hesam Yarmohammadi [a], Masoud Esmaili [b]

[a] Faculty of Electrical Engineering, Shahid Beheshti University, Evin, Tehran, Iran
[b] Department of Electrical Engineering, West Tehran Branch, Islamic Azad University, Tehran, Iran

ARTICLE INFO

Article history:
Received 17 June 2018
Revised 4 November 2018
Accepted 22 December 2018
Available online 7 January 2019

Keywords:
Doubly Fed Induction Generator (DFIG)
Fault-Ride-Through (FRT)
Superconducting Magnetic Energy Storage (SMES)
Superconducting Fault Current Limiter (SFCL)
Hybrid Big Bang Big Crunch (HBB-BC)

ABSTRACT

Wind farms equipped by Doubly-Fed Induction Generators (DFIG) should have two capabilities so that system operators can efficiently utilizes them. These capabilities include Fault-Ride-Through (FRT) and smoothing the output active power fluctuations, especially when these generators provide significant electrical power. The Superconducting Fault Current Limiter (SFCL) and also the Superconducting Magnetic Energy Storage (SMES) are supplementary devices which are used to enhance these capabilities and reduce electrical power swings. In the present work, improvement of FRT capability and smoothing the output power of wind farms are formulated as a multi-objective problem in a fuzzy framework. The variables of optimization are the Proportional-Integral (PI) gains of DFIG and SMES controllers and also SMES and SFCL parameters. Minimization of the initial energy stored in the SMES unit, the energy losses of SFCL, deviations of the DC-link voltage of DFIG, deviations of output active power of DFIG, deviations of output voltage of DFIG, and DFIG speed deviations are six objective functions of the problem. These objective functions are scaled by a fuzzy operator, then the scaled objective functions are aggregated by the "max-geometric mean" operator to obtain the multi-objective function. For optimizing this multi-objective function, the Hybrid Big Bang Big Crunch (HBB-BC) as a meta-heuristic optimization algorithm is used. The proposed algorithm is implemented on a case study to numerically evaluate its efficiency. Simulation results show that the proposed algorithm is more effective to enhance FRT capability and smooth output power of wind farm in comparison with the other algorithms.

1. Introduction

Nowadays, due to the rapid growth of renewable energies and wind power, it is essential to analyze their effects on electrical power systems. It is estimated that the installed capacity of wind power will reach 200 GW by the end of 2020, an increase of 20% compared to the previous year [1]. In many wind farms, Doubly-Fed Induction Generators (DFIGs) are used due to their benefits including simple installation, low cost, and good controllability of the active and reactive power [2]. However, the wind turbine equipped by Doubly-Fed Induction Generators (DFIGs) deals with the problems of the fluctuations of output power as well as Fault-Ride-Through (FRT).

By occurring a fault in a power system, a high value of induced voltage and current in the rotor-side converter is generated due to the sudden change in the DFIG bus voltage [3]; such overcurrent and overvoltage can damage the converter. The outage of DFIG may solve this problem; nevertheless, the power system stability can be endangered by the separation of DFIG wind farms [4]. The ability of wind farm to overcome this condition without disconnecting the DFIGs is called the FRT capability that can be improved using Superconducting Fault Current Limiter (SFCL) [5]. Despite controlling DFIG to achieve maximum electrical power, the variation of wind speed leads to fluctuations in the output electrical power of DFIG. These oscillations can be alleviated using Superconducting Magnetic Energy Storage (SMES) [5].

So far, a few research works have been carried out to enhance FRT capability and smoothing electrical power oscillations in wind farms by SMES and SFCL. In [6], a Fault Current Limiter-Battery Energy Storage System (FCL-BESS) is proposed for enhancing the dynamic response of DFIG against changing wind speed and occurring a grid fault. Satisfying the FRT requirements from both the grid-side and the DFIG is proposed by [7] employing a resistive-type SFCL which is connected in series with the DFIG rotor. Reference [5] proposes optimal parameter tuning of the SMES-FCL which have the superconducting coil (SC) as a common part for

* Corresponding author.
E-mail address: m_sedighi@sbu.ac.ir (M. Sedighizadeh).
Peer review under responsibility of Karabuk University.

https://doi.org/10.1016/j.jestch.2018.12.013
2215-0986/

improving FRT capability and smoothing output power. Ref. [8] proposes a SMES controlled by a fuzzy logic controller and hysteresis current controller to augment the dynamic response of a wind turbine based on DFIG in case of events. A coordinated optimal control of a resistive type SFCL and a SMES is proposed by [9] to enhance the FRT capability and smooth power fluctuation of DFIG-based wind farms. In this work, some parameters of the SFCL as well as the SMES are simultaneously optimized so that the initial energy stored in the SMES coil, the sudden rise in the kinetic energy of the DFIG rotor in case of events, the energy loss of the SFCL, and the output power oscillations of the DFIG are minimized. Ref. [10] improves the transient stability of the DFIG in wind farms by a non-superconductor FCL (NSFCL) based on the diode-bridge. Ref. [11] enhances the FRT of the DFIG for a 20 MW wind farm by a non-linear controller based on new bridge type fault current limiter (NC-NBFCL). Ref. [12] introduces a fuzzy logic controlled parallel resonance fault current limiter (FLC-PRFCL) to support the DFIG to improve FRT capability during temporary symmetric and asymmetric faults. Ref. [13] introduces a sensitivity index based on the terminal voltage of the wind farm for improving the transient stability of a multi-machine power system integrated with a SMES and a wind farm based on DFIG. Ref. [14] proposes an approach to enhance the dynamic response of DFIG for frequency control of an interconnected two-area power system by coordinated control of thyristor controlled phase shifter (TCPS) which are series with the tie-line and SMES.

In the previous works, the optimal coordinated control of only SMES and SFCL is considered to enhance FRT performance and smooth output active power of DFIG: gains of DFIG controllers are taken into account as constant values. In contrast, in the present work, the optimal coordinated control of DFIG, SFCL, and SMES as well as tuning of optimal parameters of SMES and SFCL are simultaneously performed. In this paper, the enhancement of FRT and flattening the output active power of DFIG are formulated as Multi-Objective Problem (MOP) with six objective functions. These objective functions play an important role in the operation of a power system equipped by SMES and SFCL. A fuzzy operator is used to scale the objective functions within the range of [0, 1] and the max-geometric mean operator aggregates the scaled objective functions. The MOP is solved by Hybrid Big Bang Big Crunch (HBB-BC) as a meta-heuristic optimization algorithm that joints PSO and BB-BC algorithms. This algorithm is based on intelligent computing techniques and has a high convergence rate in comparison to other meta-heuristic optimization algorithms. The main contributions of this paper can be mentioned as follows:

- Using SMES and SFCL optimal controllers for improving the FRT capability and alleviating active power oscillations.
- Performing the coordinated control of DFIG, SFCL, and SMES simultaneously.
- Considering six objective functions including the initial stored energy in the SMES unit, the energy loss of SFCL, deviations of the DC-link voltage of DFIG, deviations of output active power of DFIG, deviations of output voltage of DFIG, and DFIG speed deviations.
- Scaling the objective functions by a fuzzy operator and aggregating them by the max-geometric mean operator.
- Implementing the HBB-BC algorithm on the proposed MOP.

The following organization is considered for this paper. Section 2 represents dynamic model of the system. Then, the problem formulation is discussed in Section 3. Afterwards, Section 4 explains the proposed algorithm. Then, the numerical results are elucidated in Section 5 and finally, conclusions are presented in Section 6.

2. Dynamic model of the system

In Fig. 1, a typical system of DFIG connected to SFCL is shown where it is connected to a 220 kV transmission line through a 0.69/35 kV and a 35/220 kV transformer. In bus 1, a SMES is connected in order to prevent active power fluctuations of DFIG [15].

2.1. Dynamic modeling of DFIG

The presented model of DFIG in this work is shown in Fig. 2. In this figure, the DFIG model consists of two converters including the Rotor-Side Converter (RSC) and Grid-Side Converter (GSC) [16]. In Fig. 2, β is the pitch angle and V_w is the wind speed that are input signals for DFIG.

2.1.1. RSC control

Fig. 3 illustrates RSC controllers. It can be observed that the RSC converter has four Proportional-Integral (PI) controllers totally having eight proportional and integral gains. These gains are a part of optimization variables.

With respect to Fig. 3, I_{sabc} and V_{sabc} are three-phase stator currents and voltages, respectively, and θ_s and $\rho_s$are the phase of stator voltage and phase of the stator flux, respectively. I_{sabc} is the three-phase rotor currents and $\rho_s$can be formulated as:

$$\rho_s = tan^{-1}\left(\frac{\lambda_{\beta s}}{\lambda_{\alpha s}}\right) \tag{1}$$

where $\lambda_{\alpha s}$ and $\lambda_{\beta s}$ are the stator flux transferred to the $\alpha\beta$ reference frame. It can be observed that the rotor speed ω_r is compared to the reference of rotor speed ω_r^* and the resultant is inserted to PI_1 whose output makes i_{qr}^*. The reactive power of stator calculated by the Power Calculation box Q_s, is compared to the reference one Q_s^* and the resultant is inserted to the PI_3 whose output makes i_{dr}^*. After that, the q-axis rotor current i_{qr} is compared to the reference one i_{qr}^* and the resultant is inserted to the PI_2 whose output makes V_{qr1}. Then, the d-axis rotor current i_{dr} is compared to the reference one i_{dr}^* and the resultant is inserted to the PI_4 whose output makes V_{dr1}. After adding V_{qr1} and V_{dr1} with V_{qr2} and V_{dr2}, the results are labeled by V_{qr} and V_{dr} which are transferred to the *abc* frame and the resultant signal is inserted to the Pulse Wide Modulation (PWM) in order to produce a control signal for RSC. The V_{qr2} and V_{dr2} can be calculated as:

$$V_{dr2} = -s\omega_s\sigma L_r i_{qr} \tag{2}$$

$$V_{qr2} = s\omega_s\left(\sigma L_r i_{dr} + L_m^2\frac{i_{ms}}{L_s}\right) \tag{3}$$

$$\sigma = 1 - \frac{L_m^2}{L_s L_r} \tag{4}$$

$$i_{ms} = \frac{V_{qs} - r_s i_{qs}}{\omega_s L_m} \tag{5}$$

2.1.2. GSC control

Fig. 4 exemplifies RSC controllers. It can be seen that the GSC converter has four PI controllers with totally eight proportional and integral gains. These gains are also a part of optimization variables. The controller illustrated by Fig. 4 can stabilize the DC- link voltage and also alleviate fluctuations in the stator voltage which is generated by changing the wind speed.

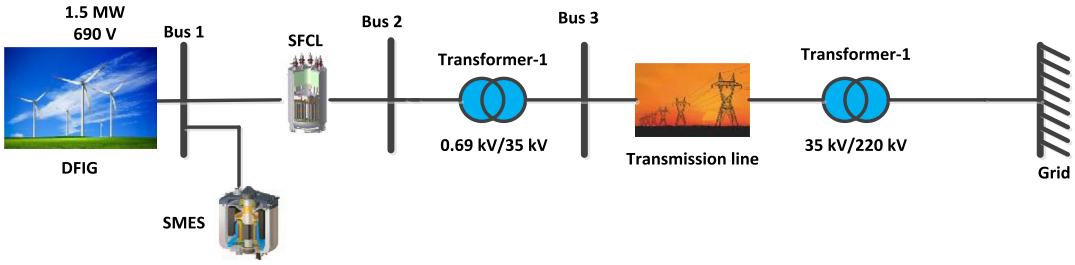

Fig. 1. Power system model.

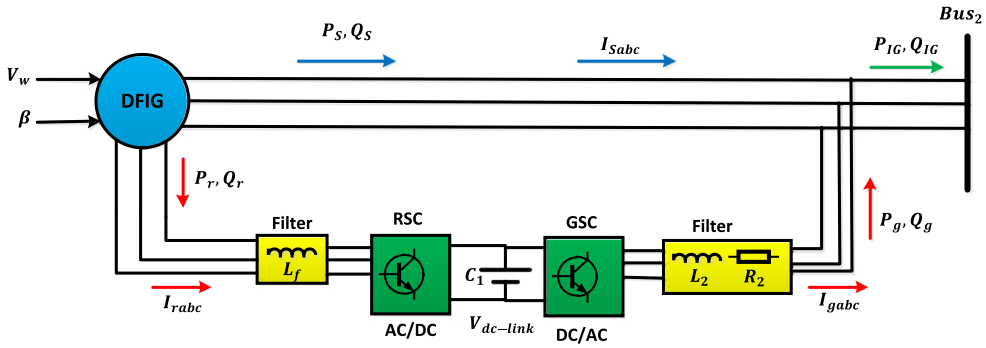

Fig. 2. DFIG Model.

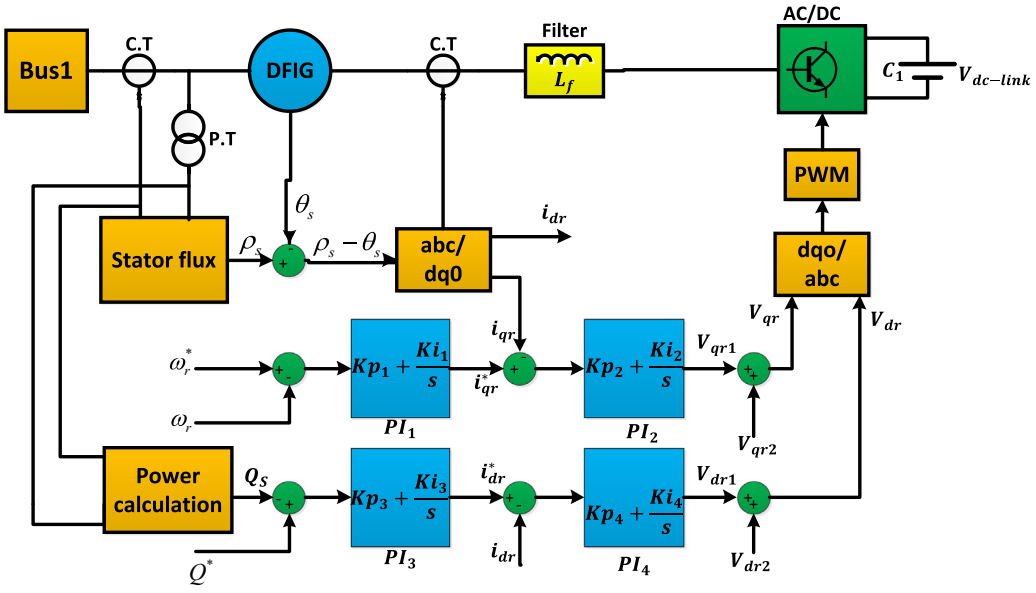

Fig. 3. RSC controller.

2.2. SMES control

The structure of the SMES along with its control is shown in Fig. 5. The SMES structure includes a DC/DC converter, a DC link capacitor, and a superconductor coil with an inductance. The Voltage Source Inverter (VSI) is controlled by PWM through five PI controllers presented in the Fig. 5 [4]. These controllers act in the *dq* reference fame; therefore, the proposed structure have two *abc*/*dq* transformations. The phase of the transformed voltage from three-phase voltages to *d*-*q* axis voltages that is necessary for *abc*/*dq* conversion is provided by Phase-Locked Loop (PLL). In this paper, the PI gains of these four controllers are a part of optimization variables and are optimally determined.

2.3. SFCL model

The proposed SFCL structure has a flexible resistance so that it has no resistance in normal conditions but it produces a high resistance in case of faults to limit the fault current and prevent the sudden overcurrent and voltage dip in the DFIG [17]. The resistance reduces to its initial value of zero during post-fault. This period is called the heat operation. The SFCL resistance value varies as follows:

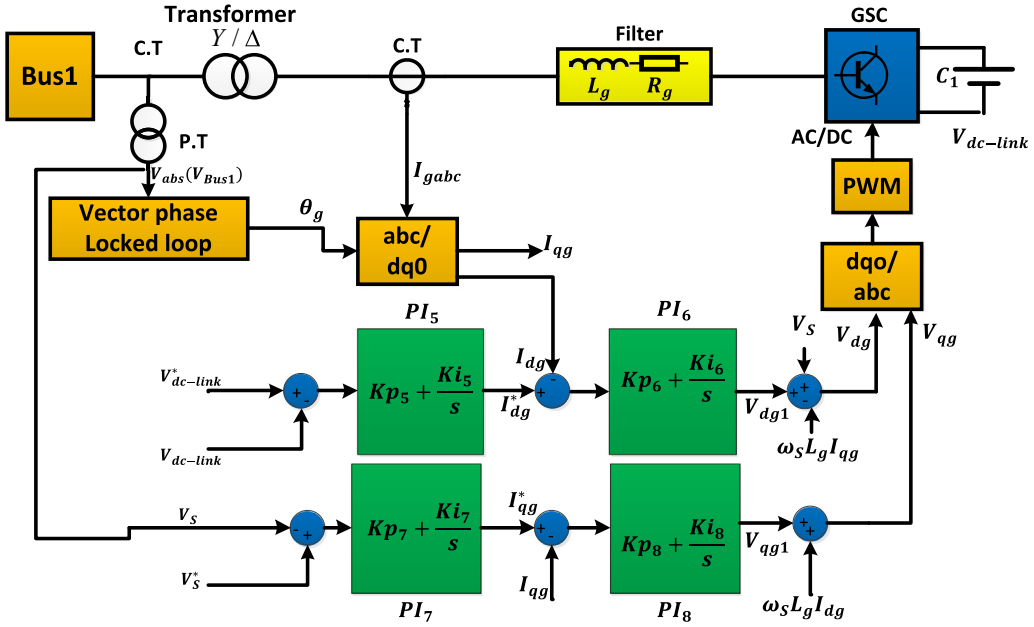

Fig. 4. GSC controller.

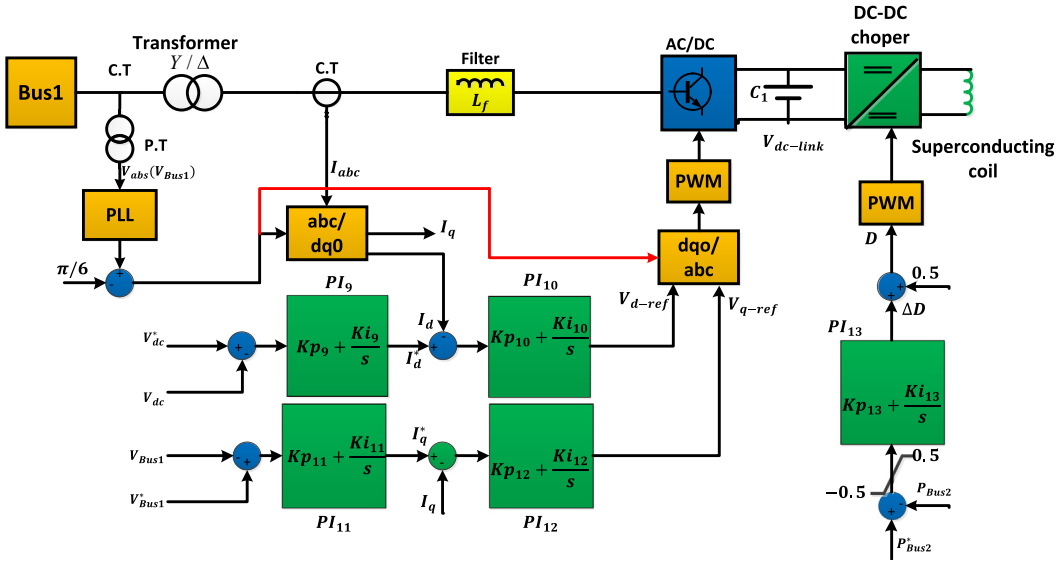

Fig. 5. The control structure for SMES.

$$R_{SFCL}(t)=\begin{cases}0 & t<t_0\\ R_m\left(1-exp\left(\frac{-t}{\tau_1}\right)\right) & t_0\le t<t_1\\ R_m & t_1\le t<t_2\\ R_m\left(exp\left(\frac{-t}{\tau_2}\right)\right) & t_2\le t<t_3\\ 0 & t\ge t_3\end{cases} \tag{6}$$

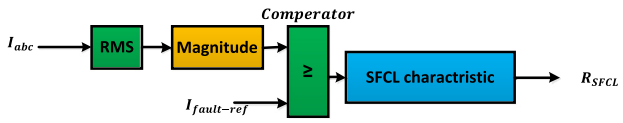

Fig. 6. The control structure for SFCL.

where R_m is the maximum SFCL resistance during the heat operation; τ_1 is time constant of the first period; τ_2 is time constant of the second period that are considered as 1 and 50 ms, respectively; t_0 is the start time of fault; t_1 is the time of first period to reach to maximum resistance; t_2 is the time of dealing with fault; t_3 is the time of the second period to reach the resistance to zero from its maximum value. The SFCL structure used in this paper is shown in Fig. 6.

In this model, the three-phase current $I_{a,b,c}$ are firstly measured and then, the RMS block computes the Root Mean Square (RMS) current which is compared to the reference of fault current $I_{fault-ref}$. Whenever the RMS current exceeds $I_{fault-ref}$, a signal 1 is given to the SFCL characteristic block and SFCL starts to action.

3. Problem formulation

In order to augment the FRT capability and smooth the active power fluctuations, six objective functions are taken into consideration to make a MOP. These objective functions are the minimization of the initial stored energy in the SMES unit, the energy loss of SFCL, deviations of the DC-link voltage of DFIG, deviations of output active power of DFIG, deviations of output voltage of DFIG, and DFIG speed deviations. The optimization variables of the MOP include PI gains of DFIG and SMES controllers, resistance of SFCL, initial current and inductance of SMES. These objective functions are formulated as follows.

3.1. Minimization of the initial energy stored in SMES

The initial stored energy in SMES is calculated as follows:

$$E_{SC0} = \frac{1}{2} L_{SC} I_{SC0}^2 \tag{7}$$

where E_{SC0}, L_{SC}, and I_{SC0} are initial stored energy in SMES, inductance, and initial current of SMES, respectively. Consequently, the objective function is defined as follows:

$$Ming_1 = \frac{E_{SC0}}{E_{SC0_0}} \tag{8}$$

where E_{SC0_0} is initial stored energy in SMES before optimization.

3.2. Minimization of energy loss of SFCL

The energy loss of SFCL can be obtained as:

$$E_{SFCL} = \int_{t_0}^{t_C} R_m i(t)^2 dt \tag{9}$$

where $i(t)$is current of SFCL, R_m is maximum resistance of SFCL; t_0 and t_C are the time of inserting fault and the clearing fault, respectively.

Therefore, the objective function can be calculated as:

$$Ming_2 = \frac{E_{SFCL}}{E_{SFCL_0}} \tag{10}$$

where E_{SFCL_0} is the energy loss of SFCL before optimization.

3.3. Minimization of deviations of terminal voltage of DFIG

Here, the Integral of Absolute Error (IAE) of terminal voltage deviations is considered as the other objective function.

$$IAE_{V_{t=}} \int_0^{\infty} |e(t)| dt \tag{11}$$

where $e(t) = \Delta V_t$. Thus, the objective function is obtained as follows:

$$Ming_3 = \frac{IAE_{V_t}}{IAE_{V_t 0}} \tag{12}$$

where $IAE_{V_t 0}$ is IAE of terminal voltage deviations before optimization.

3.4. Minimization of rotor speed deviations

The *IAE* of rotor speed is taken into account as criterion for rotor speed deviations which can be obtained as:

$$IAE_{\omega=} \int_0^{\infty} |e(t)| dt \tag{13}$$

where $e(t) = \Delta\omega$. Therefore, the objective function is defined as follows:

$$Ming_4 = \frac{IAE_{\omega}}{IAE_{\omega 0}} \tag{14}$$

where $IAE_{\omega 0}$ is IAE of rotor speed deviations before optimization.

3.5. Minimization of deviations of the DC-link voltage of DFIG

The IAE of the DC-link voltage deviations is considered as the other objective function.

$$IAE_{V_{dc-link=}} \int_0^{\infty} |e(t)| dt \tag{15}$$

where $e(t) = \Delta V_{dc-link}$. Thus, the objective function is obtained as follows:

$$Ming_5 = \frac{IAE_{V_{dc-link}}}{IAE_{V_{dc-link}0}} \tag{16}$$

where $IAE_{V_{dc-link}0}$ is IAE of the DC-link voltage deviations before optimization.

3.6. Minimization of active power deviations in the DFIG bus

The IAE of active power deviations in the DFIG bus is considered as the other objective function.

$$IAE_{P=} \int_0^{\infty} |e(t)| dt \tag{17}$$

where $e(t) = \Delta P_{bus2}$. Thus, the objective function is obtained as follows:

$$Ming_6 = \frac{IAE_P}{IAE_{P0}} \tag{18}$$

where IAE_{P0} is IAE of the active power deviations in DFIG bus before optimization.

3.7. Obtaining the overall fuzzy satisfaction degree

Given that in this paper the main goal is to simultaneously minimize all objective functions, it is necessary to use a MOP technique to solve the problem. This is due to the fact that the objectives may conflict with each other and optimizing one of them will not lead to optimize the others. There are several methods to combine objective functions. Since the objective functions have different ranges, one of the most suitable methods for scaling them is to use fuzzy membership functions. In the fuzzy scaling, each objective function is scaled as a real number within the span of [0, 1] by a trapezoidal membership function. The membership function for objective function i is formulated as:

$$\varphi_i = \begin{cases} 1 & g_i \le g_i^{min} \\ \frac{g_i^{max} - g_i}{g_i^{max} - g_i^{min}} & g_i^{min} < g_i < g_i^{max} \\ 0 & g_i \ge g_i^{max} \end{cases} \tag{19}$$

where g_i^{min} and g_i^{max} are the lower and upper bound of objective function i; g_i is the value of objective function i to be scaled; μ_i is the membership corresponding to g_i.

Due to this fact that all six objective functions should be minimized, the minimum value of objective function i (g_i^{min}) is occurred by minimization of it individually notwithstanding of other objective functions. Therefore, each of five objective functions must be minimized as a single-objective optimization problem to obtain g_i^{min} values. Besides, the maximum value among the five single-objective optimization solutions are taken into account as g_i^{max}

values. Trying to determine the range of objective functions in multi-objective problems is called the payoff table method [18].

The objective functions scaled by fuzzy memberships are combined using the "max-geometric mean" technique. It is expressed as [19]:

$$\varphi = (\varphi_1.\varphi_2.\varphi_3.\varphi_4.\varphi_5.\varphi_6)^{1/6} \tag{20}$$

where, φ is taken into account as the fitness function of multi-objective functions. The maximization of the overall membership function in (20) optimizes all objective functions simultaneously. The objective function proposed by (20) should be optimized with considering the constraints of PI controller with SMES and SFCL parameters bounds as follows:

$$R_m^{min} \le R_m \le R_m^{max} \tag{21}$$

$$I_{SC0}^{min} \le I_{SC0} \le I_{SC0}^{max} \tag{22}$$

$$L_{SC}^{min} \le L_{SC} \le L_{SC}^{max} \tag{23}$$

$$K_{Pi\_min} \le K_{Pi} \le K_{Pi\_max} \qquad i = 1, 2 \cdots, 13 \tag{24}$$

$$K_{Ii\_min} \le K_{Ii} \le K_{Ii\_max} \qquad i = 1, 2 \cdots, 13 \tag{25}$$

where K_{Pi_min}, K_{Ii_min}, K_{Pi_max} and K_{Ii_max} are the lower and upper limits of the PI controller parameters and $R_m^{min}, R_m^{max}, I_{SC0}^{min}, I_{SC0}^{max}$, L_{SC}^{min} and L_{SC}^{max} are the lower and upper limits of the SMES and SFCL parameters, respectively.

The Lagrangian method as a mathematical tools or other meta-heuristic methods including Genetic Algorithm (GA) and Particle Swarm Optimization (PSO) can solve this optimization problem. In the next section, the HBB-BC algorithm is proposed as one of the most effective combinational meta-heuristic methods to solve the suggested problem.

4. HBB-BC method to solve the optimization problem

In this section, the HBB-BC solution method, which is developed from PSO and BB-BC, is introduced.

4.1. The Hybrid Big Bang-Big Crunch (HBB-BC) algorithm

Notwithstanding the original BB-BC algorithm [20] has the good performance to search local optimum, it is deficient to obtain the global optimum in the search space. To put it more simply, it has a good performance in exploitation, yet it has no suitable capability in exploration. To solve this shortage, [21] proposes reinforcing the BB-BC algorithm abilities with those of the PSO algorithm. The combination of these two optimization algorithms as the HBB-BC algorithm not only utilizes the center of mass definition from the original BB-BC algorithm, but also generates new candidates using the PSO algorithm which provides the best position of each candidate and the global best position. This algorithm calculates the center of mass as follows [22]:

$$X_i^{C(k)} = \frac{\sum_{j=1}^{N} \frac{1}{f_j} . X_i^{(k,j)}}{\sum_{j=1}^{N} \frac{1}{f_j}} \qquad i = 1, 2, \cdots, D \tag{26}$$

where $X_i^{C(k)}$ is the entry i in the center of mass vector in iteration k; $X_i^{(k,j)}$ is entry j of candidate solution i in iteration k; f_j is the amount of fitness function for candidate j; N and D are the population size (the number of candidate solutions) and the number of decision variables, respectively. The new position of each candidate is given by [22]:

$$X_i^{(k+1,j)} = \alpha_2 X_i^{C(k)} + (1-\alpha_2)(\alpha_3 X_i^{gbest(k)} + (1-\alpha_3) X_i^{lbest(k,j)}) + \frac{r_j \alpha_1 (X_{i\,max} - X_{imin})}{k+1} \qquad i = 1, 2, \ldots, D \quad j = 1, 2, \ldots, N \tag{27}$$

where r_j is a random number obtained from the Gaussian distribution which is changing for each candidate; α_1 is a parameter to bound the size of search space; X_{imax} and X_{imin} are the upper and lower bound of the ith decision variable. In addition, α_2 and α_3 are parameters which adjusts the role of global optimum and local optimum on new position of candidates, respectively; $X_i^{lbest(k,j)}$ specifies the best position of particle i until iteration k; $X_i^{gbest(k)}$ express the best position among all candidates up to iteration k.

A mutation operator assures that the HBB-BC algorithm is not converged to local optimums. This operator is formulated as:

$$X_i^{(k+1,j)} = X_{imin} + rand() \times (X_{imax} - X_{imin}) if\ rand() < P_m \tag{28}$$

where P_m is the mutation probability which is generated in the range of [0,1]. The $P_m$closer to 1, the higher number of particles will have mutation; $rand()$ is a random number between [0,1] with uniform distribution.

4.2. Termination criteria

The criteria for termination of proposed algorithm should be taken into account either as the maximum number of iterations or convergence of the algorithm to a desired fitness value. Fig. 7 exemplifies the flowchart of the proposed algorithm in this regard. After identifying parameters of proposed algorithm and providing initial populations, the fitness function for particles is computed by (20). Then, the center of mass is calculated by (26) and next, updating the best global position and the best local positions of particles are carried out. Finally, the algorithm updates the candidate positions and applies the mutation operator by (27) and (28), respectively. The procedure will continue until the criterion of the termination is satisfied.

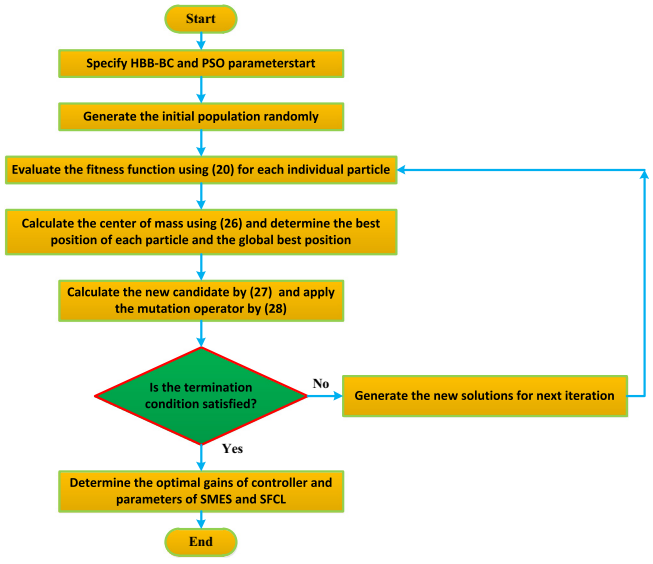

Fig. 7. Flowchart of the proposed algorithm.

5. Numerical results

In order to assess the ability of proposed algorithm to solve the above-mentioned MOP in comparison to other metaheuristic algorithms, the simulation results obtained by HBB-BC are compared in this section to those computed by using PSO algorithm. Given that scaling the single objective functions by (19) needs the best and worst values of objective functions that are calculated through single objective optimization, in the first step of simulations, the optimization is carried out as single objective. After that, the scaled objective functions are aggregated by (20) and the problem is solved as MOP. Finally, the proposed method is examined by using the time domain analysis to ensure the proposed controller correctly operates in response to system disturbances. It should be noted that the simulations performed in this paper were implemented using the MATLAB (R2015b) software on a computer with Intel Core i5 2.50 GHz CPU. The parameters of the under study system are given in [16].

The initial parameters selected for optimization algorithms for PSO and HBB-BC are presented in Table 1. These parameters is determined based on a trial and error approach with an initial point which is defined with respect to the implementation of them in the other applications [21,23]. Also, the range of the variations of optimization variables is given in Table 2.

5.1. Single-objective optimization

In order to evaluate the efficacy of the suggested optimization algorithm, objective functions are individually optimized. Given the random nature of the proposed and PSO algorithm, these algorithms are run for 30 times, and the statistical results of HBB-BC are compared to those obtained by the PSO algorithm as shown in Table 3. The disturbance applied to system is a three-phase short-circuit with the impedance 1 Ω in bus 2 which happens at $t = 0.4$s and is cleared after 100 ms. By analyzing the simulation results in Table 3, it is clear that the HBB-BC algorithm provides better results in comparison to the PSO algorithm for each of the objective functions.

Table 1
The initial parameters selected for PSO and HBB-BC algorithms.

HBB-BC		PSO	
Parameters	Values	Parameters	Values
α_1,α_2	1, 0.5	ω_{min}	0.005
α_3	0.75	ω_{max}	0.05
P_m	0.2	C_1, C_2	0.09, 0.1
PopSize	20	*PopSize*	20
Max Iteration	10	*Max Iteration*	10
Max Trial	30	*Max Trial*	30

5.2. Multi-objective optimization

This subsection presents simulation results for MOP. The fitness function is formulated as (19) and optimization variables are the gains of PI controllers as well as SMES and SFCL parameters. Table 4 shows the optimal values of gains and parameters obtained by the proposed algorithm in comparison to those calculated by the PSO algorithm.

As Table 4 implies, the optimal value proposed by the HBB-BC algorithm for SFCL resistance is 0.0953 Ohm, which is less than 0.112 Ohm of the PSO algorithm. It causes less voltage drop in the power system. Likewise, the SFCL energy for the proposed algorithm is equal to 1.831MJ, which is less than 2.724MJ of the PSO. The SMES inductance and current are 3.2113H and 783A, respectively, which are less than those of the PSO algorithm and thus, the SMES energy reduces to 1.0265MJ, which is significantly less than 1.3221MJ of the PSO algorithm. The reduction of energy in SFCL and SMES reduces the operational costs as well as investment costs.

Fig. 8 illustrates convergence trends for the proposed algorithm in comparison to the PSO algorithm to show the ability of the proposed algorithm. As it is observed, the proposed and PSO algorithms reach their final value of objective function in 44 and 54 iterations, respectively. Therefore, the proposed algorithm has a

Table 4
The multi objective optimization by HBB-BC and PSO algorithm.

Parameters	HBB-BC	PSO
K_{P1}, K_{I1}	8.011, 0.332	8.429, 0.353
K_{P2}, K_{I2}	7.912, 7.631	7.234, 7.241
K_{P3}, K_{I3}	8.991, 0.457	8.657, 0.467
K_{P4}, K_{I4}	0.742, 6.332	0.627, 6.756
K_{P5}, K_{I5}	0.075, 0.637	0.069, 0.634
K_{P6}, K_{I6}	0.322, 0.821	0.427, 0.765
K_{P7}, K_{I7}	0.248, 1.991	0.345, 1.345
K_{P8}, K_{I8}	9.071, 4.693	9.745, 4.234
K_{P9}, K_{I9}	1.723, 4.639	1.956, 4.237
K_{P10}, K_{I10}	2.967, 4.853	2.625, 4.123
K_{P11}, K_{I11}	0.546, 3.468	0.427, 3. 217
K_{P12}, K_{I12}	0.328, 3.271	0.368, 3. 874
K_{P13}, K_{I13}	2.194, 0.549	2.827, 0.442
$R_m(Ohm), I_{SC0}(KA), L_{SMES}(H)$	0.0953, 0.783, 3.211	0.112, 0.807, 3.857

Table 2
The range of the variations of optimization variables.

$R_m(Ohm)$		$L_{SC}(H)$		$I_{SC0}(KA)$		K_P		K_I	
R_m^{min}	R_m^{max}	L_{SC}^{min}	L_{SC}^{max}	I_{SC0}^{min}	I_{SC0}^{max}	K_P^{min}	K_P^{max}	K_I^{min}	K_I^{max}
0.01	2	0.001	5	0.1	5	0.0001	10	0.0001	10

Table 3
The single objective optimization by HBB-BC and PSO algorithm for 30 trails.

Objective function	HBB-BC				PSO			
	Best solutions	Worst solution	Mean	St. dev.	Best solutions	Worst solution	Mean	St. dev.
$g_1(pu)$	0.6735	1.8951	1.2843	0.4892	0.9872	2.3431	1.6512	0.7453
$g_2(MJ)$	0.2492	1.8574	0.9505	0.8073	0.3713	2.8348	1.6459	0.9602
$g_3(pu)$	0.0166	0.1843	0.1005	0.0768	0.1534	1.1762	0.6453	0.0965
$g_4(rad/sec)$	1.2239e−3	3.3899e−3	2.306e−3	1.0382	1.7562e−3	3.7892e−3	2.256e−3	1.0798
$g_5(pu)$	0.01762	0.1429	0.0803	0.0672	0.0192	0.1856	0.0987	0.0934
$g_6(pu)$	0.0748	1.6284	0.8516	0.6678	0.0954	1.8973	0.8765	0.7689

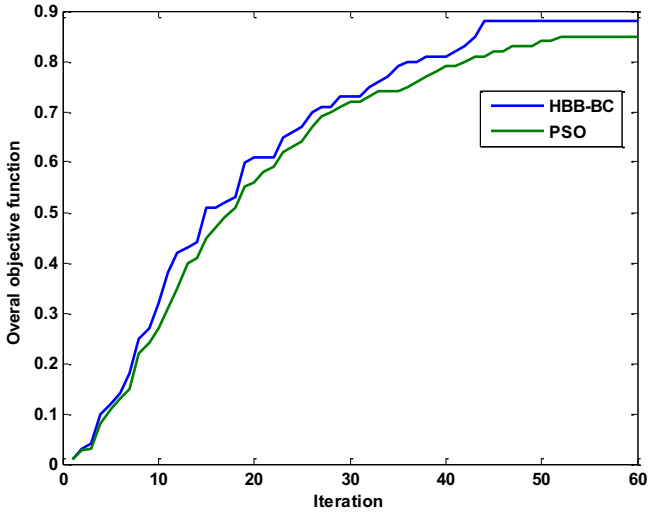

Fig. 8. The convergence curves for proposed algorithm in comparison to PSO algorithm.

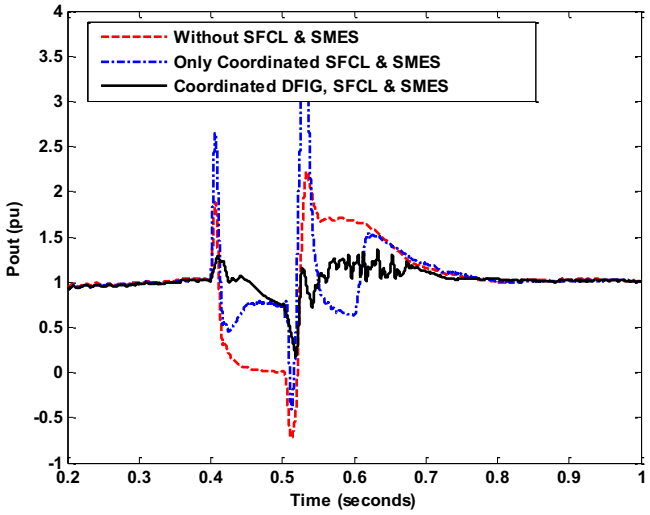

Fig. 9. The active power of DFIG.

higher convergence rate compared to the PSO algorithm. In addition, the HBB-BC algorithm has higher convergence accuracy in comparison to PSO. This is due to the fact that the final value of objective function for HBB-BC algorithm stands higher than that of the PSO algorithm. The higher convergence rate and accuracy of the proposed algorithm compared to other algorithms make it a promising method to be used in real-time applications. It should be noted that the average time taken to achieve the optimal value of fitness function by the PSO and proposed algorithms are 33 and 28 s, respectively.

5.3. Time domain simulations

In this subsection, time domain simulation results are performed for various operation conditions. In this simulation, it is supposed that a three-phase fault to ground with the impedance 1 Ω happens at $t = 0.4$ s at bus 2 (Fig. 1) and it is cleared at $t = 0.5$ s. The simulation results are illustrated in three scenarios as follows:

Scenario 1: Without considering SFCL and SMES
Scenario 2: Considering non-optimized DFIG controllers and SFCL and SMES optimized by HBB-BC
Scenario 3: Considering DFIG, SFCL, and SMES controllers optimized by HBB-BC

The response of the system to this event for three scenarios such as the output active and reactive power of DFIG generator, the DC-link voltage of DFIG, terminal voltage of DFIG, and the rotor speed are shown as Figs. 9–13. As Fig. 9 implies, the active power reaches zero during the fault in the first scenario, while the active power drop reduces with applying the optimized SMES and SFCL for the second and third scenarios. During the post-fault, the active power oscillations and overshot are reduced in scenario 3. Fig. 10 displays the reactive power output of the DFIG. It can be seen that the minimum reactive power is consumed by DFIG in the scenario 3. Fig. 11 demonstrates the DC-link voltage of DFIG. Excessive overvoltage in the DC-link cause instability of DFIG as well as damaging the DFIG converters. It can be observed that in the first scenario, the voltage value reaches about 1.9pu, while in the third scenario, it just reaches about 1.2pu, and consequently, the third scenario has the least variations during the fault and post-fault. Fig. 12 shows the terminal voltage of DFIG. It can be seen that the Low

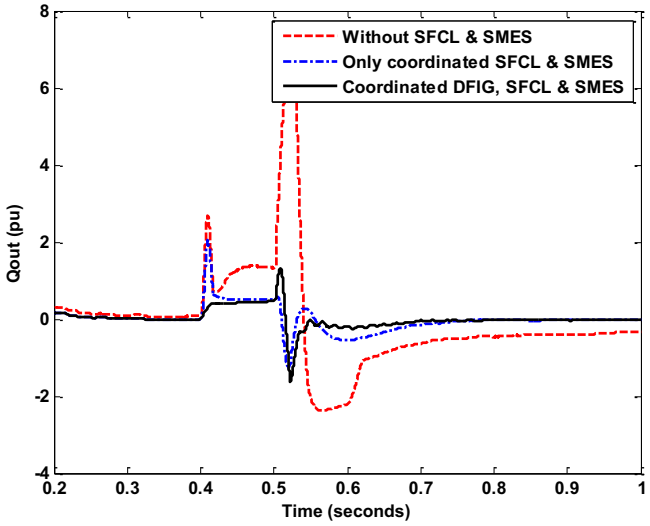

Fig. 10. The reactive power of DFIG.

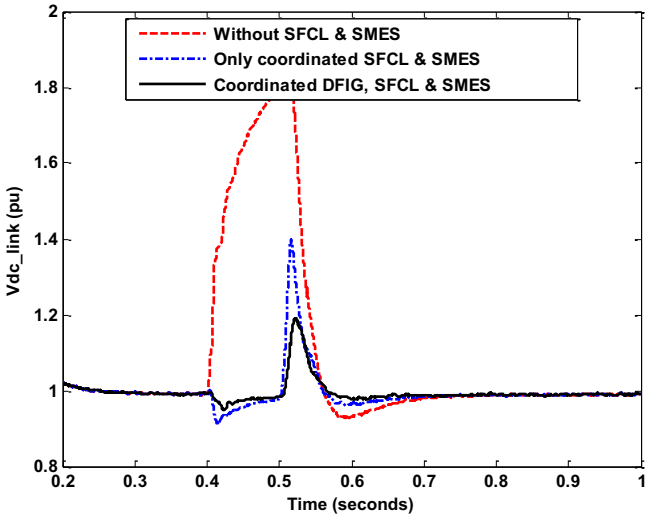

Fig. 11. The DC-link voltage of DFIG.

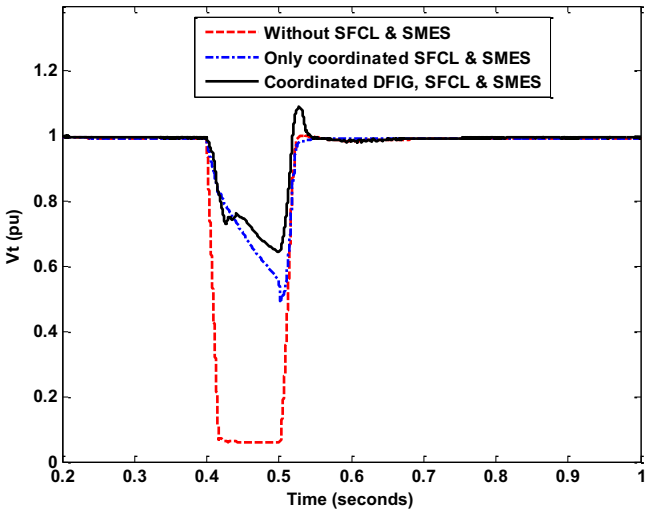

Fig. 12. The terminal voltage of DFIG.

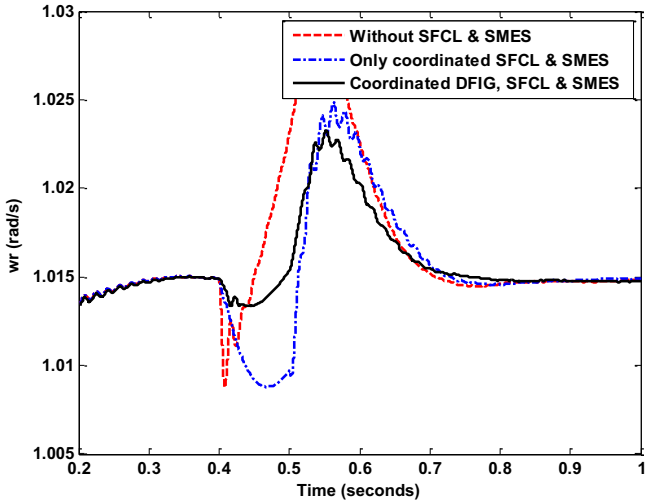

Fig. 13. The rotor speed of DFIG.

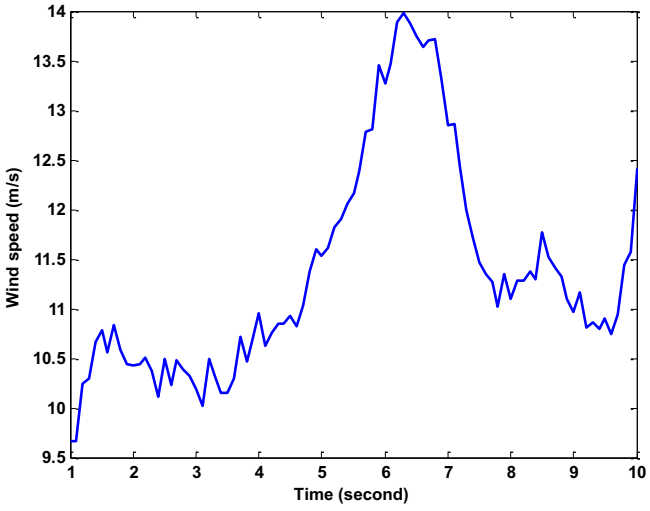

Fig. 14. The wind speed pattern.

Voltage Ride Through (LVRT) capability is enhanced by using optimal coordination of DFIG, SFCL, and SMES simultaneously. These optimal controllers prevent the extensive voltage drop and cause that voltage remains in the permissible range. Fig. 13 exemplifies the rotor speed of DFIG. Applying optimal settings prevents the over speed of DFIG and improves FRT capability.

The performance of these devices for electrical power smoothing is evaluated by a wind speed pattern as displayed in Figs. 14 and 15 that depicts the output power of DFIG considering the wind pattern. It can be seen that without considering SMES and SFCL, the output power drastically changes. However, the output power variations is decreased by simultaneous optimal DFIG, SFCL, and SMES parameters. Fig. 16 displays that output power fluctuations of DFIG initiated by wind speed are smoothed only by SMES operation, so that, it charges and discharges its active power at the appropriate times. However, the SFCL has no efficient role for smoothing active power. This due to this fact that the SFCL cannot actuate with variation of wind speed.

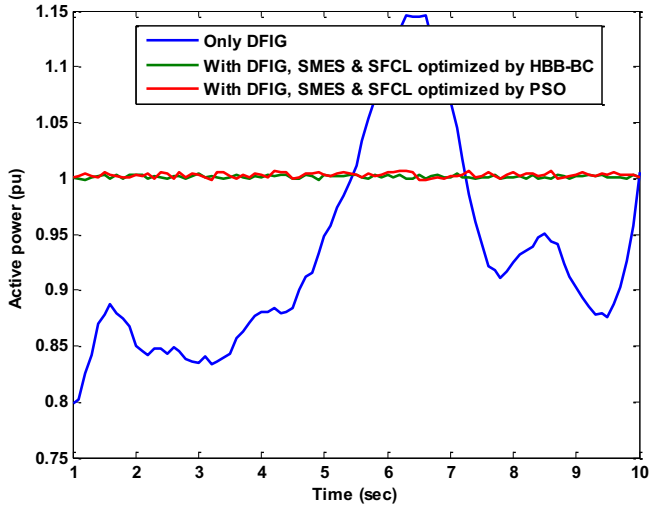

Fig. 15. The active power of DFIG.

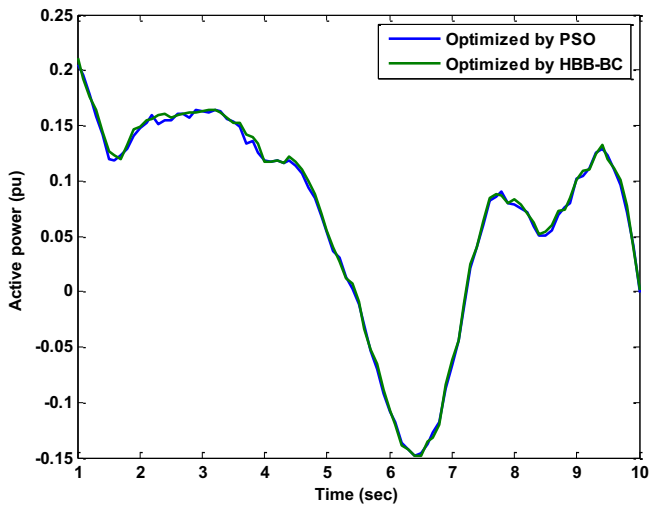

Fig. 16. The active power of SMES.

6. Conclusions

In this paper, an influential optimization algorithm for multi-objective optimization is used to enhance FRT and smoothing output power of DFIG. In order to prove the superior performance of the proposed HBB-BC algorithm in comparison to the PSO algorithm, six objective functions considered for this problem are optimized by proposed and PSO algorithms as MOP. To demonstrate the desired performance of the optimal controllers, the test system is simulated by inserting and clearing a three-phase fault with and without considering SMES and SFCL optimal controllers and variation of wind speed. The simulation results confirm that to improve FRT and to smooth output power oscillations, the proposed algorithm efficiently and quickly converge to the best optimal solutions in comparison to PSO. Finally, the proposed HBB-BC algorithm achieves a more efficient performance than PSO in single and multi-objective optimizations. In addition, the proposed algorithm reduces the SFCL losses along with SMES and SFCL energies, so that the SMES energy reaches from 1.3231MJ to 1.0265MJ and the SMES energy reaches from 2.724MJ to 1.831MJ.

References

[1] Y. Yang, H. Wang, A. Sangwongwanich, F. Blaabjerg, Design for reliability of power electronic systems, in: Power Electronics Handbook (Fourth Edition), Elsevier, 2018, pp. 1423–1440.
[2] W.-T. Liu, Y.-K. Wu, C.-Y. Lee, C.-R. Chen, Effect of low-voltage-ride-through technologies on the first Taiwan offshore wind farm planning, IEEE Trans. Sustain. Energy 2 (2011) 78–86.
[3] T. Karaipoom, I. Ngamroo, Optimal superconducting coil integrated into DFIG wind turbine for fault ride through capability enhancement and output power fluctuation suppression, IEEE Trans. Sustain. Energy 6 (2015) 28–42.
[4] I. Ngamroo, T. Karaipoom, Improving low-voltage ride-through performance and alleviating power fluctuation of DFIG wind turbine in dc microgrid by optimal SMES with fault current limiting function, IEEE Trans. Appl. Supercond. 24 (2014) 1–5.
[5] I. Ngamroo, Optimization of SMES-FCL for augmenting FRT performance and smoothing output power of grid-connected DFIG wind turbine, IEEE Trans. Appl. Supercond. 26 (2016) 1–5.
[6] W. Guo, L. Xiao, S. Dai, Fault current limiter-battery energy storage system for the doubly-fed induction generator: analysis and experimental verification, IET Gener. Transm. Distrib. 10 (2016) 653–660.
[7] Z.-C. Zou, X.-Y. Chen, C.-S. Li, X.-Y. Xiao, Y. Zhang, Conceptual design and evaluation of a resistive-type SFCL for efficient fault ride through in a DFIG, IEEE Trans. Appl. Supercond. 26 (2016) 1–9.
[8] A.S. Yunus, M.A. Masoum, A. Abu-Siada, Application of SMES to enhance the dynamic performance of DFIG during voltage sag and swell, IEEE Trans. Appl. Supercond. 22 (2012) 5702009–5702010.
[9] I. Ngamroo, T. Karaipoom, Cooperative control of SFCL and SMES for enhancing fault ride through capability and smoothing power fluctuation of DFIG wind farm, IEEE Trans. Appl. Supercond. 24 (2014) 1–4.
[10] M.E. Hossain, Performance analysis of diode-bridge-type non-superconducting fault current limiter in improving transient stability of DFIG based variable speed wind generator, Electr. Power Syst. Res. 143 (2017) 782–793.
[11] M.E. Hossain, A non-linear controller based new bridge type fault current limiter for transient stability enhancement of DFIG based Wind Farm, Electr. Power Syst. Res. 152 (2017) 466–484.
[12] G. Rashid, M.H. Ali, Fault ride through capability improvement of DFIG based wind farm by fuzzy logic controlled parallel resonance fault current limiter, Electr. Power Syst. Res. 146 (2017) 1–8.
[13] A. Mitra, D. Chatterjee, A sensitivity based approach to study the stability of the power systems integrated with wind farm and superconducting magnetic energy storage, IFAC-PapersOnLine 48 (2015) 560–565.
[14] P. Bhatt, S. Ghoshal, R. Roy, Coordinated control of TCPS and SMES for frequency regulation of interconnected restructured power systems with dynamic participation from DFIG based wind farm, Renewable Energy 40 (2012) 40–50.
[15] T. Ackermann, Wind Power in Power Systems, Wiley Online Library, 2005.
[16] W. Qiao, W. Zhou, J.M. Aller, R.G. Harley, Wind speed estimation based sensorless output maximization control for a wind turbine driving a DFIG, IEEE Trans. Power Electron. 23 (2008) 1156–1169.
[17] B.C. Sung, D.K. Park, J.-W. Park, T.K. Ko, Study on a series resistive SFCL to improve power system transient stability: modeling, simulation, and experimental verification, IEEE Trans. Ind. Electron. 56 (2009) 2412–2419.
[18] S. Chandra, A. Aggarwal, On solving matrix games with pay-offs of triangular fuzzy numbers: certain observations and generalizations, Eur. J. Operational Res. 246 (2015) 575–581.
[19] M. Sedighizadeh, R. Bakhtiary, Optimal multi-objective reconfiguration and capacitor placement of distribution systems with the Hybrid Big Bang–Big Crunch algorithm in the fuzzy framework, Ain Shams Eng. J. 7 (2016) 113–129.
[20] O.K. Erol, I. Eksin, A new optimization method: Big Bang–Big Crunch, Adv. Eng. Software 37 (2006) 106–111.
[21] M. Sedighizadeh, M. Esmaili, M. Esmaeili, Application of the hybrid Big Bang-Big Crunch algorithm to optimal reconfiguration and distributed generation power allocation in distribution systems, Energy 76 (2014) 920–930.
[22] A. Kaveh, S. Talatahari, Size optimization of space trusses using Big Bang–Big Crunch algorithm, Comput. Struct. 87 (2009) 1129–1140.
[23] A.E. Moarref, M. Sedighizadeh, M. Esmaili, Multi-objective voltage and frequency regulation in autonomous microgrids using Pareto-based Big Bang-Big Crunch algorithm, Control Eng. Pract. 55 (2016) 56–68.